



Interaction of Injector Design, Bubble Size, Flow Structure, and Turbulence in Ladle Metallurgy

Kwaku B. Owusu, Tim Haas, Prince Gajjar, Moritz Eickhoff, Pruet Kowitwarangkul, and Herbert Pfeifer

In ladle metallurgy, the flow of purge gas through injectors promotes an effective mixing of the melt concerning composition and energy. In this work, different types of gas injectors, positioned eccentrically at 66% of the ladle radius are investigated in terms of the bubble size distribution, the resultant flow field velocity, and turbulent kinetic energy. The experiments are carried out in a 1:3 scale water model of a 185 t ladle using Particle Image Velocimetry (PIV) and image processing. It is shown that a porous plug provides more intensive bulk convection and a higher degree of turbulence than the other tested injectors. The differences are explained by the generation of smaller bubbles, which transfer more momentum into the liquid. The differences between the injectors are small, though. Thus, it is concluded that in comparison with other process parameters, the type of injector plays a minor role in the efficiency of ladle metallurgy.

is among other factors determined by the gas flow rate, plug position, bath height, and slag layer. Hence, a comprehensive understanding of these factors is essential for effective process control and possible process optimization.

Many studies report the major process variables relevant to gas stirred ladle metallurgy and consequently their influences under real ladle operations are now known with a considerable level of accuracy.^[2] Independently, different studies have indicated that the gas flow rate is the key determinant in providing sufficient stirring energy while limiting slag eye formation.^[2,3] It is also evident that plug position is not negligible when optimizing the steel refinery operation. Nunes et al.^[4] observed that better mixing is obtained

1. Introduction

With the ever-increasing demand for high-quality steel, primarily in high-tech applications, ladle metallurgy has gained attention in a number scientific studies. Nevertheless, the complex process is still not fully understood. Ladle refining is used for purposes of temperature homogenization, desulphurization, degassing, adjustment of alloying elements as well as inclusion removal. During this process, argon gas is injected into the molten steel from the bottom part of the ladle through one or a number of porous plugs. The argon disintegrates into gas bubble column(s), known as plumes. Due to the buoyancy force, the bubbles rise and escape the melt through the free surface at the top.^[1,2] As they rise, the bubbles induce a recirculation flow in the ladle, that provides effective mixing. The mixing efficiency

when the porous plug is positioned eccentrically at mid-radius. It has also been found that mid-radius is the most favorable positioning for single and dual plug bubbling.^[2] In contrast, Li et al.^[5] investigated different plug positions and observed that mixing time decreases with increasing plug's radial distance. They also found that a maximum wall stress occurs at a radial plug position of 0.67 R, while a radial plug position of 0.73 R induced a different flow field which reduced the wall shear stress. Multiple plugs located diametrically opposite at mid-bath radius have proven to provide good recirculation and significantly shorter mixing time.^[6] Domgin et al.^[7] and Freire et al.^[8] established a firm connection that plugs positioned close to one another or ladle walls produces deflecting plumes, known as "Coanda effect". Evidence also exists that higher bath depth provides better circulation and tends to reduce mixing time.^[9] In addition, the height of the molten liquid determines the size of the slag-eye opening in the ladle. A lower bath depth is likely to cause a larger slag eye-opening, consequently exposing a larger area of the molten metal surface to the atmosphere. Cloete et al.^[10] reported that an increased bath depth tends to provide higher kinetic energy influx per volume of the stirring gas and reduced viscous dissipation in the plume region.

Different injector designs are in use, although their influence on the process performance has not been quantified yet. The gas injector design is responsible for the determination of bubble evolution, regime, and diameter.^[11] These gas bubble phase interactions can alter the flow pattern and influence the flow characteristics of the entire liquid bath. Understanding the impact of different gas injector designs on the flow velocity, turbulent

K. B. Owusu, P. Gajjar, P. Kowitwarangkul
The Sirindhorn International Thai-German Graduate School of Engineering (TGGS)
King Mongkut's University of Technology North Bangkok (KMUTNB)
1518 Pracharat 1 Rd., Wongsawang, Bangsue, Bangkok 10800, Thailand
E-mail: kwaku.b-pe2016@tggs.kmutnb.ac.th
K. B. Owusu, T. Haas, M. Eickhoff, P. Gajjar, Prof. H. Pfeifer
Department for Industrial Furnaces and Heat Engineering (IOB)
RWTH Aachen University
Kopernikusstraße 10, 52074 Aachen, Germany
E-mail: haas@iob.rwth-aachen.de

The ORCID identification number(s) for the author(s) of this article can be found under <https://doi.org/10.1002/srin.201800346>.

DOI: 10.1002/srin.201800346

kinetic energy, and the bubble distribution would support a better understanding of the ladle performance. In a previous work, it was reported that nozzle configurations have smaller impact on the bubble velocity, liquid rise velocity, and the gas volume fraction distribution and hence not crucial to the flow recirculation in the ladle bath.^[2] The authors also noted that the injector design influences the immediate vicinity of the injector, but not the flow caused by the bubbles rising up in the plume. Similarly, it is argued that flow recirculation in industrial ladles does not rely on the porous plug, tuyere, or nozzle gas source.^[12] Trummer et al.^[13] compared hybrid, slot, and porous plug designs. Their results showed that hybrid plugs exhibited the best performance at low and high gas flow rates among the tested plug designs. However, only a limited discussion of the flow field velocity and bubble size distribution was given. The application of the Digital Particle Image Velocimetry (PIV) measurement system to understand the flow field velocity in the ladle is also limited.

To close gaps in the understanding of the ladle operation, this study aims to provide a better understanding of the bubble size distribution, flow field velocity, and turbulent kinetic energy for different types of gas injectors as revealed by the physical modeling and PIV measurements.

2. Experimental Section

2.1. Physical Simulation

Direct measurements are difficult to conduct in industrial steelmaking plants due to the extreme conditions associated with the operation.^[14] The high temperature of about 1600 °C, visual opacity coupled with the large size of industrial ladle hinder close variable measurements and monitoring of the dynamics in the melt; henceforth empirical study of the operations become very complex and costly.^[2,15,16] However, an air-water physical model that replicates the industrial ladle processes has proven to provide a comprehensive understanding of the real system,^[14] since molten steel and water at room temperature have nearly equivalent kinematic viscosity.^[2,17] In this study, an acrylic glass model of a 185 t ladle, geometrically downscaled by a scaling

factor of three, is used. **Table 1** provides the detailed physical dimension, operating parameters and key properties of the fluid of both the industrial ladle and the scale model.

2.2. Ladle Description

The experiment is designed to physically simulate and investigate the flow field velocity, turbulent kinetic energy, and bubble size distribution resulting from different gas injector configurations. The model is built with transparent acrylic glass, at a reduced scale of 1:3 of the industrial ladle nominal capacity of 185 tons. It is slightly conical in geometry with an upper diameter of 1.11 m, lower diameter of 1.05 m, and height of 1.31 m. The model yields an aspect ratio (H/D_{mean}) of 0.9954. The water model experimental set-up is designed with three different plug positions: one centrally located plug and two plugs located diametrically opposite each other at the 0.35 m ladle radius position. In this study, only the one plug position at 0.35 m of the ladle radius is used.

2.3. Gas Injector

In the current study, five different PVC plate configurations, as well as a standard porous plug are investigated. Each plate has multiple orifices and is fixed on top of a porous plug made of mullite ceramic ($3\text{Al}_2\text{O}_3 \cdot 2\text{SiO}_2$) to maintain homogeneous outflow conditions. **Table 2** provides the geometry of the gas injectors and **Figure 1** depicts the schematic image of the plate types used in the study.

2.3.1. Similarity Criteria

Physical simulation can be used to predict the flow behavior in the real ladle. However, the size of bubbles measured in the water model is not typically representative of the real ladle situation because 1) the wettability of water and liquid steel with

Table 1. Employed physical properties (steel in ladle at 1600 °C, water model, scale 1:3 at 20 °C).

Property	Unit	Industrial Ladle	Water model
Steel/water density	kg m ⁻³	6932	998
Steel/water viscosity	Pa · s	5.06×10^{-3}	1×10^{-3}
Kinematic viscosity	m ² s ⁻¹	0.91×10^{-6}	1×10^{-6}
Injected gas	-	Argon	Compressed air
Dispersed gas density	kg m ⁻³	0.83	1.2
Internal diameter	m	Max. 3.34, Min. 3.15	Max. 1.11, Min. 1.05
Gas flow rate	slm	200	8.3, 16.7, 25, 33.3, 41.7, 50
Aspect ratio(H/D_{mean})	-	0.9954	0.9954
Liquid height	m	3.23	1.08
Full liquid volume	m ³	2.967	0.989
Porous plug diameter	mm	270	90
Plug eccentricity, e	m	1.05	0.35

Table 2. Geometry of the gas injectors employed.

Case number	Description	Number of orifices	Orifice diameter, d_o [mm]	Orifice spacing, s_o [mm]
1	Standard porous plug with a thin plate ring	-	-	-
2	Porous plug fixed with a plate to reduce the diameter	1	70	-
3	Porous plug fixed with a plate of 1 mm orifices	5 × 5	1	15
4	Porous plug fixed with a plate of 2 mm orifices	5 × 5	2	15
5	Porous plug fixed with a plate of 3 mm orifices	5 × 5	3	15
6	Porous plug fixed with a plate of 2 mm orifices in a single line	5	2	15

porous plugs differs, 2) the density gradient and surface tension between the bulk liquid and gas are different, and 3) the thermal expansion of the bubbles is not considered in the water model. Therefore, complete gas–liquid reaction similarity between the water model and industrial ladle is difficult to predict. Notwithstanding this constraint, the air–water model still provides acceptable qualitative results that could support a better understanding in the real ladle situation.^[18] From the literature,^[19] the following dependence of the bubble diameter on the surface tension and the mass density is known:

$$d_g \approx \sqrt{\frac{\sigma_{g,f}}{(\rho_f - \rho_g)g}} \quad (1)$$

The similarity criteria of the gas bubble diameter between the water model and the industrial ladle can be assumed as:

$$d_{g,B} = d_{g,M} \cdot \sqrt{\frac{\sigma_B (\rho_f - \rho_g)_M}{\sigma_M (\rho_f - \rho_g)_B}} \quad (2)$$

where d_g = gas bubble diameter, σ = surface tension, ρ_f = density of fluid, ρ_g = density of gas, g = gravity, $d_{g,B}$ = gas bubble diameter of plant, $d_{g,M}$ = gas bubble diameter of model, M = model (water/air), and B = Plant (steel/argon).

Equation (2) is derived for an equilibrium. Thus, it does not take the nucleation and bubble growth mechanisms at the injectors take into account. Consequently, Equation (2) can only be a rough estimate for the actual bubble size.

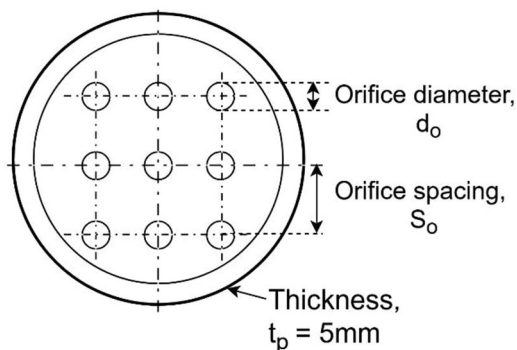


Figure 1. Schematic view of plate design and configurations.

2.4. Method

The 1:3 scale water model was placed in an outer rectangular tank ($134 \times 134 \times 148 \text{ cm}^3$) constructed from acrylic glass for two basic reasons^[2,16]: 1) to mechanically stabilize the ladle model by balancing the pressure between the two tanks when filled with water; and 2) to minimize the influence of refraction on the visual observations of the ladle's curved walls. Both tanks (ladle model and rectangular tank) were filled with water at room temperature at the same time until the desired filling height was obtained. The plug was connected to a mechanical mass flow controller (Krohne DK800) and pressure regulator (Riegler 737.313) to allow for the adjustment of the volume flow rate of the stirring gas at 2 bar. The mass flow controller works on a float measuring principle. The measuring unit consists of a calibrated glass cone in which a float, which freely moves up and down was manually adjusted to achieve the desired flow rate. The gas expands in the liquid because the surrounding pressure is lower. Thus, the actual volume flow rate through the plug is higher. Each plug was investigated using six different gas flow rates, Q , namely 8.3, 16.7, 25, 33.3, 41.7, and 50 slm.

A PIV system was used to measure the steady state velocity flow field resulting from the use of the different injector configurations. It utilizes a double-pulsed Nd: YAG laser to expose the images and a digital image recording device, which is the Charge-Coupled Device (CCD) double frame camera with a resolution of 2048×2048 . The delay time between the double frames was $22\,000 \mu\text{s}$. Before the measurement, the water in the ladle was seeded with fluorescent tracing particles (Rhodamine B, $10\text{--}20 \mu\text{m}$). Rhodamine B has a fluorescent wavelength of 584 nm. One major challenge was that the phase boundaries of the gas bubble have the tendency to reflect the laser light and serve as flow tracing particles. To avoid the bubbles' interference and track only the Rhodamine B particles when determining the velocity of the fluid, a cut-off filter ($>540 \text{ nm}$) was applied to the PIV camera lens. An optical device was used to spread the laser into a thin light sheet positioned at the symmetric plane of the water model so that the exposed particles are on the main flow plane. 1250 double-frames were captured with a frequency of 5 Hz for every gas injector type at the six different gas flow rates. The series of double-frames were further processed using Davis 8 evaluation software and Tecplot 360 EX 2017 R1 to determine the mean flow field velocity and the turbulent kinetic energy in the entire cold-water model. Masking, cross-correlation, peak validation, and

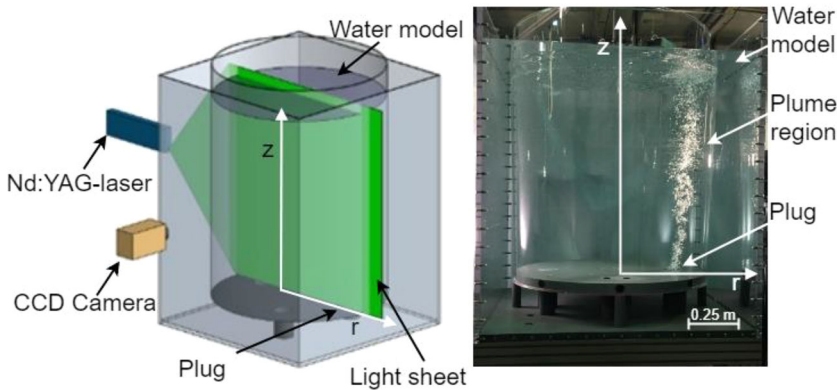


Figure 2. Experimental setup.

the mean statistics of the velocities were considered during the evaluation of the data. A schematic diagram of the experimental process is shown in **Figure 2**.

In order to measure the bubble size, a digital camera (Canon EOS 5DS, resolution: 50.6-megapixel) was used to capture images of the plume under diffuse light environment. Observation of the bubbles was limited to a section of the plume between $z = 300$ and 700 mm. The gas bubble size was analyzed with a MATLAB™ program. The program automatically encloses individual bubbles with a rectangular boundary taking into account the major and minor axes to determine the equivalent diameter. Since some bubbles were not detected while some disturbances were identified as bubbles, a manual enhancement approach was followed. Therein, wrongly identified bubbles were removed and undetected individual bubbles were identified and added to the set of correctly recognized bubbles.

3. Results

3.1. Flow Fields

The ladle flow pattern and velocity field have been studied with a cross-correlation PIV measurement technique. The PIV technique is used to visualize and compare the velocity field in the water model as a result of using different gas injectors. **Figure 3** shows a schematic of the cross section of the side view of the ladle model and a top view indicating where the cross section is taken. The visualization results of the different gas injectors at a flow rate of 25 slm and a constant filling height of 1.08 m are presented in **Figure 4**. It describes the velocity and structure of the flow field on the main flow plane (symmetric plane, $z = 0$).

It is evident that the rising gas bubble plume is the driving force behind the flow field velocity and recirculation in the entire bath. The rising bubbles exchange momentum with the fluid, causing an upward flow in the plume region, which has been quantified in **Figure 5**. The flow alters path on the free surface, descend along the sidewall from the top left corner of the bath and finally proceed horizontally at the bottom to be redirected into the plume. This creates a circulation loop and prevents the occurrences of a “dead zone” at the bottom of ladle as it was

observed by Perez et al.^[3] in the case where two injectors were employed.

In comparison, it can be seen that the flow field velocity for the various gas injectors under the same conditions are relatively different. The velocities of some regions are comparatively high while others are low. The Case 1 and Case 2 injectors produce the highest velocity, predominantly in the bottom left region, while the other injectors result in a more similar and moderate velocity in the ladle. An area exists in all flow fields, known as “dead zone” in which the velocity drops off so that the flow in this zone is almost stagnate. All flows show a small “dead zone” at the upper left corner, centered as the vortex

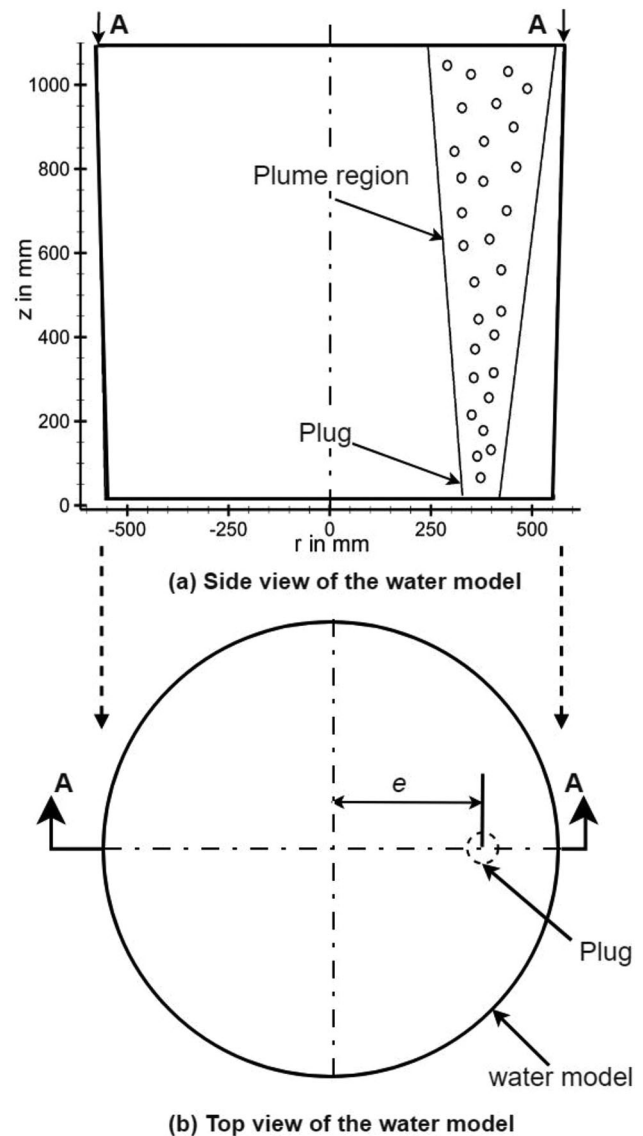


Figure 3. Schematic image showing a) cross section A-A of the ladle and b) a top view of the ladle, indicating the position of cross section A-A.

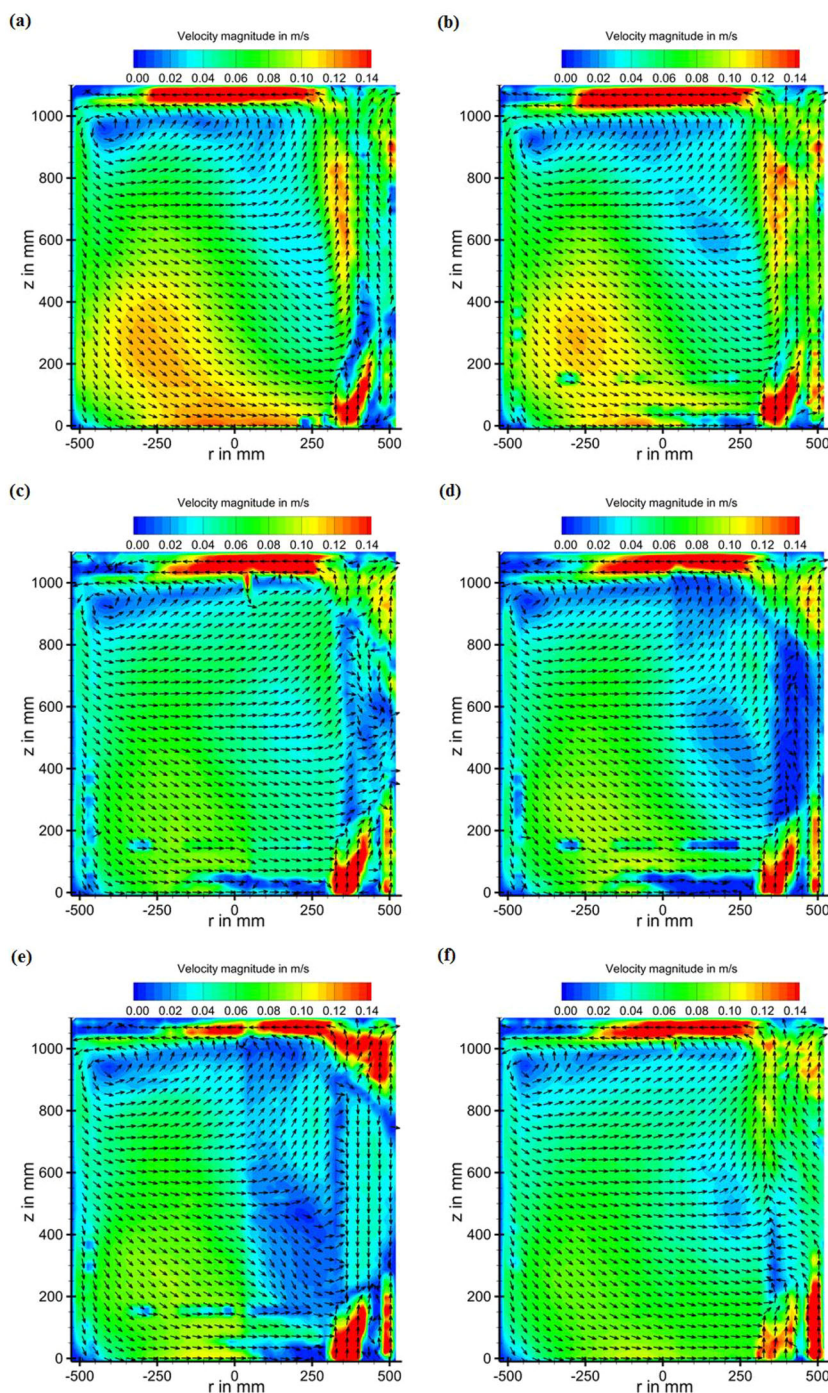


Figure 4. PIV flow pattern and contours for cross section A-A with $Q = 25$ slm for a) Case 1, b) Case 2, c) Case 3, d) Case 4, e) Case 5, and f) Case 6.

structure, which transfers the flow momentum from the free surface toward the lower parts of the ladle. Otherwise, the extent, position and number of the “dead zone” alter slightly with the injector applied. The injectors used in Case 1 and Case 2 show closely related flow structures with a similar “dead zone” in the top region, stretching out parallel to the free surface. However, the velocity magnitude in the left bottom region of the ladle is

slightly higher in Case 1, where a full diameter opening is used. The injectors used in Case 3, Case 4, Case 5, and Case 6 yield flow structures characterized mostly by homogeneous circulation. This effect is more pronounced in Case 3 and Case 6. The presence of “dead zone” is seen in the upper regions of all the cases with PIV plates. This zone is the largest in Case 4 and Case 5 and the smallest in Case 3 and Case 6.

In the plume region between $r = 300$ and 500 mm, the results of the flow velocity magnitude are evaluated separately and shown in Figure 5. Since the flow is symmetrical at the plume center, only one side of the plume is shown. According to the results, it is seen that the velocity magnitude of all the injector cases has similar patterns. The Case 1/2 shows the highest velocity magnitude followed by Case 5. Case 6 recorded the lowest velocity magnitude. However, the velocity differences in all the cases happen to be small.

3.2. Turbulent Kinetic Energy

Since the mixing within the ladle can be driven by bulk convection and eddy diffusion,^[20] the turbulent kinetic energy is also investigated as a measure for the degree of turbulence. For this purpose, the turbulent kinetic energy was derived from the PIV measurements. Because PIV measures only the flow field velocity in the 2D symmetry plane of the ladle, the TKE is also evaluated for the same plane. To estimate how the TKE is distributed inside the ladle, the raw PIV data of the velocity field are used. The TKE is estimated from the average instantaneous flow field velocity as follows^[21]:

$$E_{tke} = \frac{1}{2} |V_{rms}|^2 [m^2s^{-2}] \quad (3)$$

V_x and V_z each add a $\frac{1}{4} V_{rms}^2$

$$E_{tke} = \frac{1}{2} V_{rms}^2 + \frac{1}{4} V_{rms}^2 = \frac{3}{4} V_{rms}^2 \quad (4)$$

where E_{tke} is the TKE and V_{rms} is velocity vector fields.

The TKE provides a single value that represents the varying levels of all the velocity components at each point. The resulting TKE data are exported, analyzed and visualized by using TecPlot EX 2017 R software. The results are illustrated in Figure 6. As one would expect, the turbulent kinetic energy is the highest in regions of high flow velocities. The results from Case 1 and Case 2 are similar and show that the turbulent kinetic energy is especially high at the bottom left part of the ladle. Case 3, Case 4, and Case 6 show

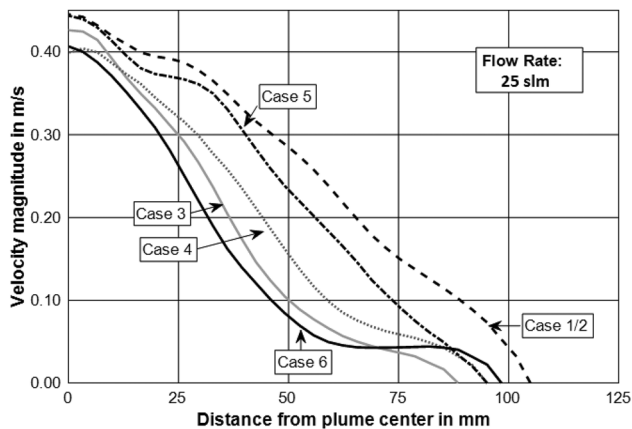


Figure 5. The plume velocity magnitude of all the injector designs at $z = 0.5$ m.

similar turbulent kinetic energy profiles. The Case 5 injector exhibits the lowest turbulent kinetic energy. Generally, the highest turbulent kinetic energy is observed in the plume region where the flow velocity is very high, the free surface, and to some extent on the left side of the ladle.

3.3. Bubble Equivalent Diameter

For the determination of the bubble size and the calculation of the equivalent diameter, a MATLAB™ script was used. The shape of plume bubbles has been identified in previous studies as spherical, ellipsoidal and spherical cap bubbles.^[22] The bubble shapes were assumed as ellipsoidal with major and minor axes, a and b respectively.^[9] The equivalent diameter, D_{eq} , was calculated using the equation:

$$D_{eq} = (d_{max}^2 \cdot d_{min})^{1/3} \quad (5)$$

where d_{max} is the major axis and d_{min} is the minor axis of the bubble.

Since almost no difference in the bubble size between the full porous plug and the reduced diameter porous plug (Case 1 and Case 2) could be observed, they are presented as one case in the presentation and interpretation of the results. **Table 3** shows the number of bubbles analyzed in each case for the respective flow rates. Only single bubbles are evaluated. At higher flow rates, clusters are formed which cannot be separated even with manual enhancement.

An increased flow rate caused an increase of the bubble density in the plume region. As a consequence, bubbles tended to be behind each other, causing clusters of overlapping bubbles on the image. Applying a smaller camera aperture value blurs out bubbles which are out of the focal plane. However, as can be seen in **Figure 7**, for some clusters, it becomes impossible, even by manually evaluating the image, to identify individual bubbles. Thus, several bubble clusters were neglected in determining the equivalent diameter. This drawback was most pronounced in case of a flow rate of 25 slm.

Figure 8 depicts the mean measured equivalent diameter in the plume region resulting from the use of different gas injector designs at different gas flow rates.

The measurements show that for all investigated flow rates the porous plug produces the smallest bubbles, although the effect declines with an increase in the flow rate. Except for the case of the porous plug, the average equivalent diameter decreases with increasing the gas flow rate. At a flow rate of 8.3 slm, the largest equivalent diameter of 7.9 mm is observed in Case 4 and the lowest of 3.4 mm in Case 1/Case 2. Concerning the highest flow rate of $Q = 25$ slm, the largest and smallest respective average equivalent bubble diameter are produced by the injector used in Case 3 with an equivalent diameter of 6.2 mm, and in Case 1/Case 2 where 4 mm bubbles are produced.

3.3.1. Bubble Frequency Distribution

To provide sufficient information to evaluate the bubble size distribution at different gas flow rates, frequency distribution profiles are derived from the bubble data. Typical results of the bubble occurrence distribution are plotted in **Figure 9**. The profiles are mostly symmetrical and show a similar “bell curve” shape for all the injector types at flow rate of 8.3, 16.7, and 25 slm. The effect of increasing the gas flow rate from 8.3 to 16.7 slm slightly widened the bell-shaped profile. Interestingly, when the gas flow rate is further increased to 25 slm, the bubble profile is somewhat narrowed again. It could be that some additional small bubbles are formed at 25 slm due to bubble collision and disintegration.

At 8.3 slm, Case 1/Case 2 produces a narrow range of bubble sizes varying between 1.4 and 6 mm with a pronounced maximum of 3.4 mm. In contrast to that, the other injectors produce a broader range of sizes with a less distinct maximum. The size variation of the injector orifices has a small effect on the frequency and size, especially in Case 3, Case 4, and Case 5. Additionally, the substantial frequency reduction in Case 6 explains the influence of the number of injector orifices on the bubble production.

By increasing the flow rate to 16.7 slm, the maxima become less pronounced and the “bell shape” widens. Interestingly, the effect slightly reverses when the flow rate is further increased to 25 slm. However, it cannot be stated conclusively whether this is a physical effect or a result of the inseparable clusters occurring at higher flow rates.

In the case of the porous plug, a large number of small nucleation sites are present. Thus, especially at low gas flow rates, most bubbles are formed as primary bubbles (“mother bubbles”) of which the size and shape are determined by the outflow of the plug. This is indicated by the narrow bubble occurrence distribution. Since the bubbles are relatively small, their size is stabilized by a high surface tension to volume ratio. Thus, coalescence and break up plays a minor role. At higher flow rates, the ratio of nucleation sites to the flow rate is lower. As a consequence, the bubble occurrence frequency distribution widens. In case of the PVC plates, the number of nucleation sites is significantly smaller, since it corresponds to the number of orifices. Owing to that, larger,

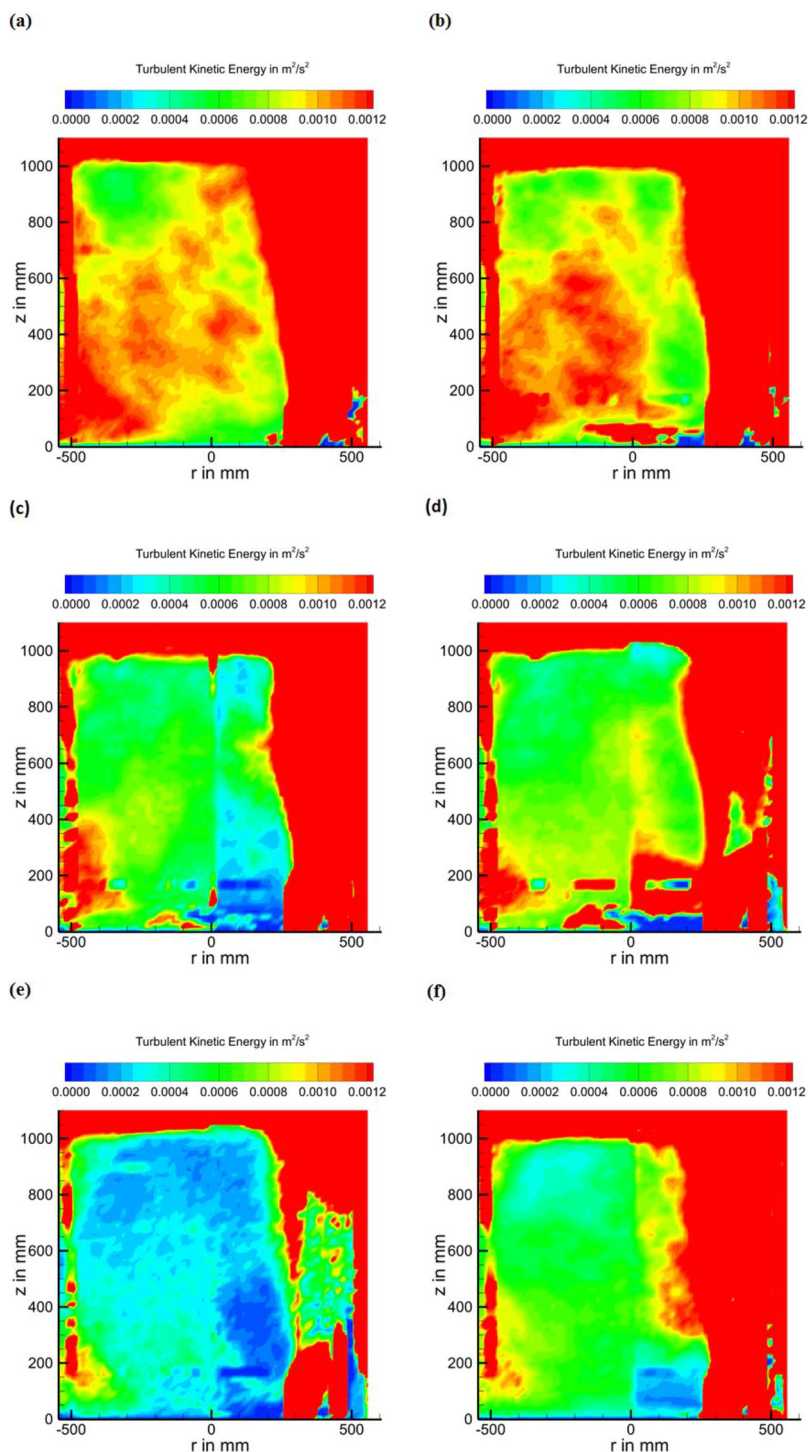


Figure 6. Turbulent kinetic energy at volume flow of 25 slm for a) Case 1, b) Case 2, c) Case 3, d) Case 4, e) Case 5, and f) Case 6.

more unstable bubbles are created which coalesce and disintegrate into smaller secondary bubbles (“daughter bubbles”). Consequently, a large number of different bubble sizes can be observed, resulting in a very broad “bell shape”.

phase present in a typical industrial steel refining process may have some level of impact on the flow pattern and mixing behavior. According to Cho et al.,^[24] the presence of a slag layer (typically presented by an oil layer in the water model)

4. Discussion

The aims of ladle metallurgy include efficient homogenization of composition and temperature. In the literature,^[18] bulk convection and turbulent diffusion were identified as decisive factors to achieve these objectives. Moreover, a circulating flow extending over the whole liquid metal and the absence of “dead zones” are preferable. The PIV measurements conducted in a 1:3 scaled water model showed that at a constant gas flow rate of 25 slm and a filling height of 1.08 m, all tested injectors deliver a good performance. Even though “dead zones” of relatively similar sizes exist for all injectors, the main circulating flow comprises the whole liquid. The most homogeneous circulating flow is obtained with the injectors used in Case 3 and Case 6. The velocity is in a similar order of magnitude for all the tested injectors, though the maximum velocity magnitude observed in case of the porous plug with full and reduced diameter exceeds the others. The turbulent kinetic energy, used as an indirect measure of the turbulent diffusion can be roughly correlated with the velocity magnitude, since the liquid’s ability to dampen turbulent disturbances in the flow declines with an increasing velocity. The highest turbulent kinetic energy could be observed in case of the porous plug, though here the absence of a diameter reduction yielded slightly higher values. Since the bulk convection and the degree of turbulence depend on one another, it cannot comprehensively be concluded which phenomenon has a larger influence on the transport in the ladle.

Comparing the PIV results with the bubble size measurements indicate that the overall momentum transfer from rising gas bubbles to the liquid is higher for smaller bubbles. Moreover, smaller bubbles are beneficial for another crucial task in ladle metallurgy, the removal of non-metallic inclusions.^[23]

In the literature, it was pointed out that a higher flow velocity in the plume region can enhance the undesirable slag eye formation.^[3] This decreases the efficiency of the ladle process since it increases the rate of reoxidation. However, the injector configuration’s impact on slag eye formation cannot be discussed based on the data, since the PIV results in the plume area are relatively close to be considered. Moreover, no top layer was used with which this effect could be examined more closely. The slag

Table 3. The number of bubbles measured in each case.

Case No.	Number of bubbles for the respective gas flow rates		
	8.3 slm	16.7 slm	25 slm
1/2	196	126	121
3	142	142	127
4	134	160	179
5	75	56	131
6	119	165	216

significantly changes the flow behavior by reducing the momentum from the rising bubbles in the plume and consequently increasing the mixing time in the ladle. It has also been shown that the slag phase dissipates some of the input energy and increases mixing time.^[2] In the absence of a slag layer, a large recirculation loop tends to form in the ladle, resulting in better mixing.^[24]

The porous plug seems to be most promising to fulfill the requirements of ladle metallurgy, since it provides the highest bulk convection and the highest degree of turbulence. It also produces the smallest bubbles, which increases the removal rate of non-metallic inclusions. The reduction of the plug diameter seems to have almost no effect.

Nevertheless, a comparison with other impact factors on ladle metallurgy, for example, the flow rate, the slag layer or the position of the plug, which were studied in multiple earlier studies, indicates that the type of injector has a minor optimizing effect on the process.

5. Conclusion

The impact of the injector design on ladle metallurgy was investigated in a 1:3 scale water model. For that, six different injectors were tested at a constant flow rate and filling height. An imaging technique was used to determine the bubble size and bubble size occurrence frequency for all injectors at different flow rates, while PIV measurements were conducted to gain insight into the convective flow and the degree of turbulence. The major findings from the investigation are:

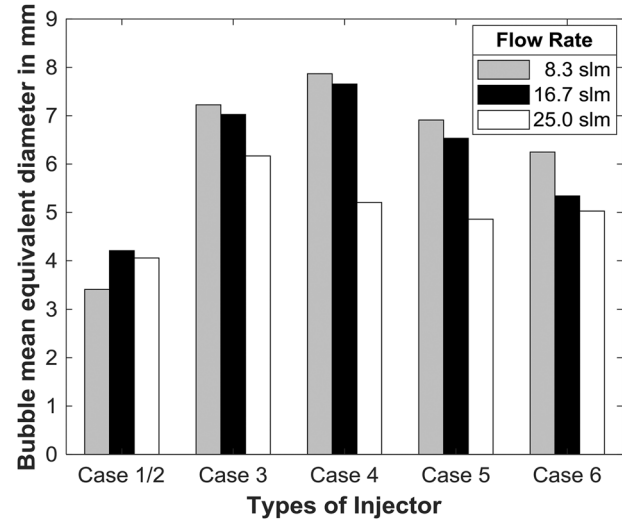


Figure 8. Mean equivalent diameter of the bubbles produced by the different gas injector designs.

- 1) The bulk convection and the turbulent kinetic energy depend on each other. Joo and Guthrie^[20] reported that the two mechanisms contribute more or less equally. The rising bubbles in the plume region play a significant role in the production of turbulence (shear and bubble induced turbulence) within the two phase plume.^[2] Moreover, the coupling of shear-induced and bubble-induced eddy fluctuations may superimpose on each other.^[25] Thus, it cannot be evaluated or quantified which phenomenon (bulk convection or turbulent kinetic energy) account for which degree of mixing.
- 2) The porous plug provides a much more uniform gas distribution due to a larger number of smaller bubbles forming. These smaller bubbles have a large interfacial contact area between the liquid and gas phases and induce more velocity than the bigger bubbles produced by the plate injectors. Therefore, they contribute to a better mixing flow condition in the ladle.

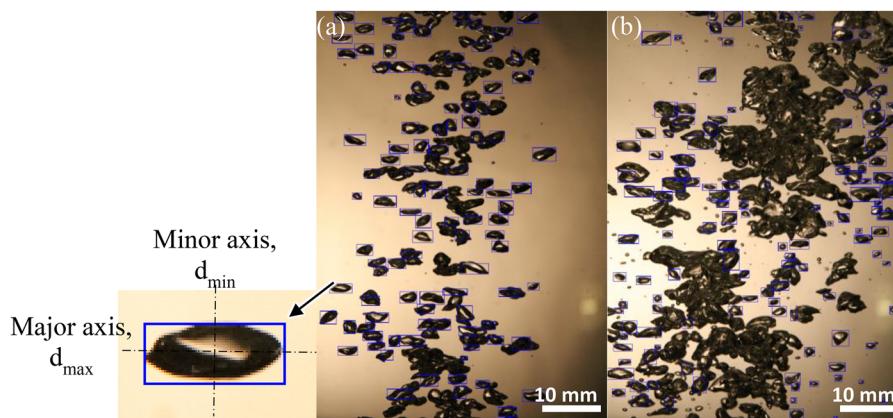


Figure 7. Bubbles recognized by the MATLABTM code on bubble images taken at a) 8.3 slm and b) 25 slm.

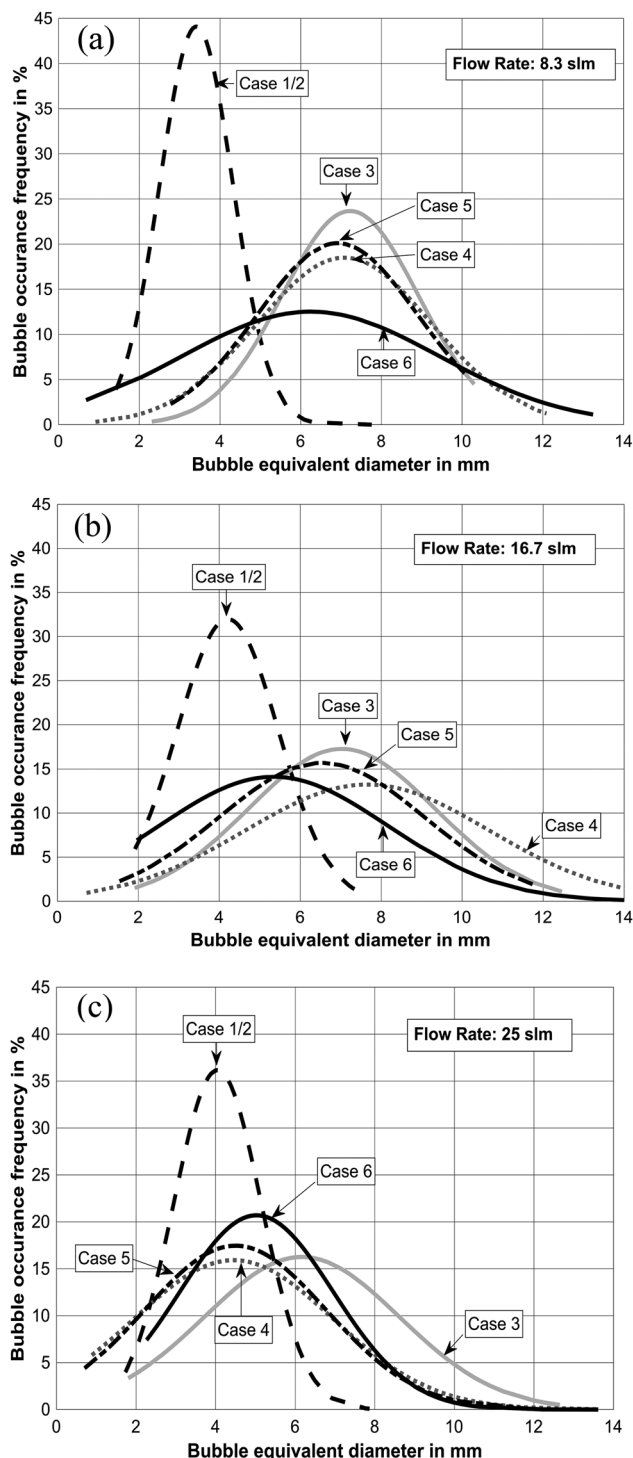


Figure 9. Bubble frequency profile at different gas flow rates a) 8.3 slm, b) 16.7 slm, and c) 25 slm.

3) The porous plug generated significantly smaller bubbles compared to the other injectors. Especially in the case of low flow rates, the size and shape of the bubbles are determined by the outflow condition of the plug, whereas coalescence

and break-up are insignificant. With increasing flow rates, these factors gain importance.

- 4) In contrast to that, the shape and size are mainly controlled by coalescence and disintegration in the case where injector plates were used.
- 5) Among the tested injectors, the porous plug seems to be best suited for the challenges of ladle metallurgy, though the differences between the injectors were small. A diameter reduction of the porous plug has a very small effect.
- 6) In comparison with other factors, the injectors effect on ladle metallurgy seems to be minor.

Abbreviations

CCD	charge coupled device
DAAD	Deutscher Akademischer Austauschdienst
DFG	Deutsche Forschungsgemeinschaft
H/D _{mean}	height of the bath melt/mean diameter of the ladle
IOB	department for industrial furnaces and heat engineering
KMUTNB	King Mongkut's University of Technology North Bangkok
RWTH	Rheinisch-Westfälische Technische Hochschule
Nd-YAG	Neodymium-doped Yttrium aluminum garnet
PIV	particle image velocimetry
PVC	polyvinyl chloride, slm, standard liter per minute
TGGS	The Sirindhorn International Thai-German Graduate School of Engineering

Acknowledgements

The authors gratefully acknowledged the support from the German Research Foundation (Deutsche Forschungsgemeinschaft (DFG)) within the project RU 2050/2-1 and acknowledged the financial assistance of the Deutscher Akademischer Austauschdienst (DAAD) and the Sirindhorn International Thai-German Graduate School of Engineering (TGGS), King Mongkut's University of Technology North Bangkok (KMUTNB), Thailand. The assistance of Suzanne Roberts (research staff, IOB, RWTH Aachen University) for carefully reading the manuscript and suggesting some corrections was greatly appreciated.

Conflict of Interest

The authors declare no conflict of interest.

Keywords

bubble size distribution, flow field velocity, injector configuration, particle image velocimetry

Received: July 4, 2018
Revised: August 24, 2018
Published online:

- [1] S. Johansen, F. Boysan, *Metall. Trans. B* **1988**, *19*, 755.
- [2] D. Mazumdar, R. I. L. Guthrie, *ISIJ Int.* **1995**, *35*, 1.
- [3] L. E. Jardón Pérez, A. A. Villeda, A. N. Conejo, C. González-Rivera, M. A. Ramírez-Argáez, *Mater. Manuf. Process.* **2018**, *33*, 882.

- [4] R. P. Nunes, J. A. M. Pereira, A. C. F. Vilela, F. T. V. Der Laan, *J. Eng. Sci. Technol.* **2007**, 2, 139.
- [5] L. Li, Z. Liu, B. Li, H. Matsuura, F. Tsukihashi, *ISIJ Int.* **2015**, 55, 1337.
- [6] Z. Liu, L. Li, B. Li, *ISIJ Int.* **2017**, 57, 1971.
- [7] J. Domgin, P. Gardin, M. Brunet, Proceedings of the Second International Conference on CFD in the Minerals and Process Industries. CSIRO, Melbourne, December **1999**.
- [8] A. P. S. Freire, D. D'E. Miranda, L. M. S. Luz, G. F. M. França, *Int. J. Multiphase Flow* **2002**, 28, 8.
- [9] K. Okumura, M. Sano, *ISIJ Int.* **2001**, 41, 234.
- [10] S. W. Cloete, J. J. Eksteen, S. M. Bradshaw, *Miner. Eng.* **2013**, 46, 16.
- [11] A. Vazquez, R. M. Sanchez, E. Salinas-Rodriguez, A. Soria, R. Manasseh, *Exp. Therm. Fluid Sci.* **2005**, 30, 49.
- [12] Y. Sahai, R. I. L. Guthrie, *Metall. Trans. B* **1982**, 13, 193.
- [13] B. Trummer, W. Fellner, A. Viertauer, L. Kneis, G. Hackl, *RHI Worldwide Bull.* **2016**, 1, 35.
- [14] C. G. Méndez, N. Nigro, A. Cardona, S. S. Begnis, W. P. Chiapparoli, *Mecán. Comput.* **2002**, 21, 2646.
- [15] S. Yu, Z. Zou, L. Shao, S. Louhenkilpi, *ISIJ Int.* **2016**, 56, 1303.
- [16] T. Haas, A. Rueckert, H. Pfeifer, 7th Int. Conference on Modelling and Simulation of Metallurgical Process in Steelmaking STEEL-SIM2017, Qingdao, August **2017**.
- [17] D. Mazumdar, P. Dhandapani, R. Sarvanakumar, *ISIJ Int.* **2017**, 57, 286.
- [18] D. Guo, G. A. Iron, *Metall. Mater. Trans. B* **2000**, 13B, 1447.
- [19] M. Neifer, *Dissertation der RWTH Aachen*, December, **1995**.
- [20] S. Joo, R. I. L. Guthrie, *Metall. Trans. B* **1992**, 23B, 765.
- [21] DaVis 8.1 manual, https://istina.msu.ru/media/equipment/files/2015/10/06/1003001_DaVis_D81.pdf, Aug. **2018**.
- [22] K. Agrawal, *J. Eng. Technol. Res.* **2013**, 5, 42.
- [23] L.-F. Zhang, S. Taniguchi, K. Matsumoto, *Iron Steelmaking* **2002**, 29, 326.
- [24] S. H. Cho, S. H. Hong, J. W. Han, B. D. You, *Mater. Sci. Forum* **2006**, 510–511, 490.
- [25] M. L. de Bertodano, R. T. Lahey, O. C. Jones, *J. Fluids Eng.* **1994**, 116, 128.